RSC Advances

PAPER

View Article Online
View Journal | View Issue

Cite this: *RSC Adv.*, 2026, **16**, 22158

Influence of the molecular adsorption of CO_2, CO and NO on the stability of oxygen vacancies on the anatase TiO_2 (101) surface

Zhi-Wen Wang, * Jie Zhang, Meng-Ting Yue, Wei-Guang Chen, Ming-Yu Zhao and Ya-Nan Tang *

The impact of the molecular adsorption of CO_2, CO and NO on the stability of oxygen vacancies at the anatase TiO_2 (101) surface is studied through first-principles calculations. Our findings reveal that the adsorption of CO_2, CO, and NO stabilizes the surface oxygen vacancy relative to the subsurface vacancy, with total energies being 0.08 eV, 0.32 eV, and 1.58 eV lower, respectively. This suggests that the adsorption of these molecules can thermodynamically reverse the relative stability between the surface and subsurface oxygen vacancies, with the surface oxygen vacancy surface becoming the most stable. Additionally, we investigate the kinetic effects of oxygen vacancy interactions with small molecules. The diffusion barriers for oxygen vacancies on surfaces with adsorbed CO_2 and CO are found to be 0.68 eV and 0.36 eV, respectively—significantly lower than the diffusion barriers on the clean surface by 0.16 eV and 0.50 eV, respectively. These results suggest that CO adsorption can effectively promote the diffusion of oxygen vacancies. Overall, this study highlights the crucial role of molecular adsorption in modulating the stability and interaction of oxygen vacancies on the anatase TiO_2 (101) surface, providing insights into the photocatalytic activity of this material.

Received 31st December 2025
Accepted 14th April 2026

DOI: 10.1039/d5ra10116f

rsc.li/rsc-advances

Introduction

Titanium dioxide (TiO_2) has been extensively studied due to its promising applications in heterogeneous catalysis, solar cells, gas sensors, photocatalysis, and environmental cleaning.[1–9] Although rutile TiO_2 is the thermodynamically stable phase, the (110) surface has been widely used as a model surface.[10–12] However, the anatase phase exhibits greater stability relative to rutile when nanoparticle dimensions are reduced below 11 nm (ref. 13), while also demonstrating superior surface reactivity.[14] Among anatase surfaces, the (101) surface is the most stable.[15] The interactions between small molecules and the TiO_2 (101) surface have been studied extensively in recent years.[16–19]

Surface oxygen vacancies (V_O^{sur}) are key defects on the TiO_2 (110) surface and play a crucial role in surface reactions.[8,11,20–27] In contrast, studies have shown that subsurface oxygen vacancies (V_O^{sub}) are more stable than surface vacancies on the anatase TiO_2 (101) surface.[26,27] As a result, there has been limited research on the interaction between small molecules and defective anatase (101) surfaces.[17–19] Notably, Setvin *et al.* reported that O_2 adsorption could reverse the relative stability of V_O^{sur} and V_O^{sub}.[17] Additionally, other studies have shown that water and methanol can facilitate the migration of oxygen vacancies (V_Os) from the subsurface to the surface on the anatase (101) surface.[18,19] We previously studied the interaction between H_2S and oxygen vacancies on the anatase TiO_2 (101) surface and found that H_2S adsorption could reverse the stability of V_O^{sur} and V_O^{sub}.[28] Upon the adsorption of small molecules such as H_2O, H_2S and methanol, V_Os on the anatase TiO_2 (101) surface undergo a stabilization transition from the subsurface to the surface layer. These V_Os can now function as accessible active sites, as they are no longer obstructed by steric hindrance or electronic screening from the surface molecular adlayer. Consequently, the decomposition of adsorbed small molecules including H_2O, H_2S, and methanol is significantly promoted, leading to an improved surface photocatalytic performance.[18,19,28]

Several important reactions occur on the anatase TiO_2 (101) surface, such as the photocatalytic reduction of CO_2 to methanol for fuel production,[16,29] low-temperature CO oxidation and CO hydrogenation reactions,[30–33] and the oxidation of NO to HNO_3 to reduce nitrogen oxide emissions from vehicles and industrial sources.[34,35] However, studies on these reactions typically overlook the stability of oxygen vacancies in the subsurface, and the effect of adsorbed molecules on the stability of oxygen vacancies is not well understood in such works. Additionally, the role of oxygen vacancies in various photocatalytic reactions remains unclear, which limits the practical application of anatase TiO_2 as a catalyst.

In this study, we systematically investigate the impact of molecular adsorption (CO_2 CO, and NO) on the stability of V_Os

College of Physics and Electronic Engineering, Zhengzhou Normal University, Zhengzhou, 450044, China. E-mail: zwwang@zznu.edu.cn; yntang2010@163.com

at the anatase (101) surface. Our results show that after CO_2, CO, and NO adsorption, the surface with V_O^{sur} becomes more energetically favorable than the surface with V_O^{sub}. This suggests that the relative stability of the surface with either a V_O^{sub} or V_O^{sur} can be reversed, with the surface containing V_O^{sur} becoming the most stable. We also examine the kinetics of V_O diffusion. We find that the diffusion barriers of V_Os from the subsurface to the surface with CO_2 and CO adsorption are only 0.68 eV and 0.36 eV, which are significantly lower than the clean surface by 0.16 eV and 0.50 eV, respectively. These findings indicate that CO adsorption can significantly enhance the diffusion of V_Os.

Computational methods

The calculations were based on density functional theory (DFT) using the Perdew–Wang 91(PW91) generalized gradient approximation[36,37] and the Vienna *ab initio* simulation package (VASP) code with projector-augmented wave pseudopotentials.[38,39] An energy cutoff of 500 eV was used for expanding the Kohn–Sham wave functions. The anatase TiO_2 (101) surface was modeled as a (1 × 4) supercell slab. The stoichiometric slab containing three O–Ti–O trilayers ($Ti_{48}O_{96}$) and a vacuum with a thickness of 20 Å, with a Γ-centered 2 × 2 mesh, has been tested to be well converged. The positions of atoms in the bottom trilayer are fixed to mimic the bulk, and the other atoms were relaxed until the forces converged to 0.01 eV $Å^{-1}$. To model a reduced anatase TiO_2 (101) surface, an oxygen atom was removed from the slab; the reduced slab contained 48 Ti atoms and 95 O atoms, and the V_O density was 1/4, which was enough for the small molecules to get adsorbed on the surface with V_Os.[28] To investigate the reaction kinetics by locating the transition states, we employed the nudged elastic band (NEB) method within the VASP framework.[40] For each elementary step, the reaction coordinate was represented by five intermediate images constructed through a linear interpolation between the boundary states. Structural relaxations along the reaction pathway were performed using the conjugate gradient scheme, with a force convergence criterion of 0.05 eV $Å^{-1}$. The reaction barrier was defined as the energy difference between the initial state to the saddle point, identified using the image with the maximum electronic energy along the minimum energy pathway.

The adsorption energy of small molecules on the TiO_2 (101) was calculated using the following equation:[41]

$$E_{ads} = E_{tot} - E_{sur} - E_{mol} - E_{ZPE} - PV + TS, \quad (1)$$

where E_{tot} is the total energy of a molecule adsorption on the slab, E_{sur} is the total energy of TiO_2 (101) surface before small molecule adsorption, E_{mol} is the energy of a molecular on a 15 × 15 × 15 $Å^3$ vacuum box, E_{ZPE} is the zero-point energy, V is the volume of the vacuum box, P and T is the relevant temperature and pressure of the box, respectively, and S is the entropy of small molecules. The chemical potentials of small molecules can be referenced to the total energy of the elementary phases at T = 0 K. The formation energies of the defects are always positive or the crystal would be unstable;[42] positive (negative) energies are intended to be an endothermic (exothermic) reaction.

Results and discussion

Our previous studies showed that the anatase TiO_2 (101) surface system containing a V_O^{sub} is more stable than that with a V_O^{sur} as the surface containing V_O^{sur} is 0.16 eV higher in total energy than the surface containing V_O^{sub}.[28] Upon introducing a V_O^{sub} into the anatase TiO_2 (101) surface, we considered thirteen potential adsorption sites for small molecules, as shown in Fig. 1a. The

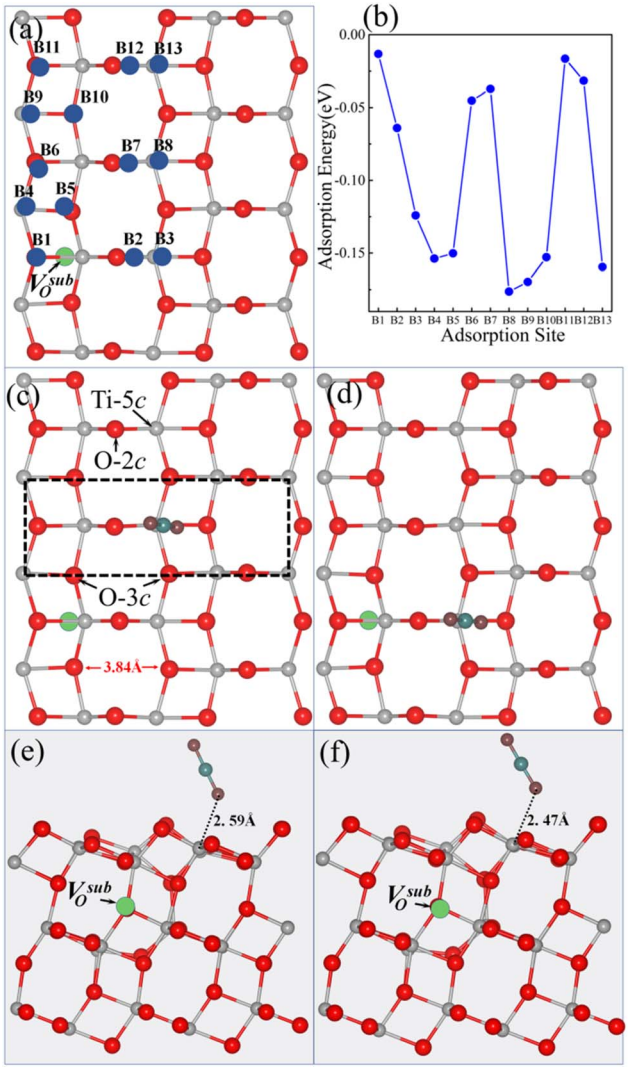

Fig. 1 (a) Top view of a 1 × 4 supercell of the anatase TiO_2 (101) surface with a V_O^{sub} and thirteen possible adsorption sites for small molecules. (b) Calculated adsorption energies of CO_2 at all the thirteen sites on the V_O^{sub}-containing surface. (c) Top and (e) side views of the optimized structure of the CO_2-adsorbed B8 site. The black dashed square in (c) outlines the primitive cell of the anatase (101) surface. (d) Top and (f) side views of the optimized structure of the CO_2-adsorbed B3 site. In the structural diagrams, gray, red, cyan, and burgundy spheres represent titanium (Ti), surface lattice oxygen (O), carbon (C), and oxygen atoms (O) from the CO_2 molecule, respectively. The green dashed circles indicate the position of the V_O^{sub}.

CO_2 molecule maintains a linear geometry; in the calculations for all the 13 adsorption sites, it was placed vertically above the surface, and the vertical distance between the lower oxygen atom of the molecule and the surface atom directly beneath the adsorption site was 1.92 Å in each case. After relaxation, the adsorption energy of CO_2 on the anatase TiO_2 (101) surface with a V_O^{sub} was calculated using eqn (1). As illustrated in Fig. 1b, the most stable adsorption site for CO_2 is the B8 site, with the optimized geometry shown in Fig. 1c and e. The most stable adsorption site corresponded to the next-nearest five-coordinated titanium atom (Ti-5c) site, where the distance between the lower oxygen atom of CO_2 and Ti-5c was 2.59 Å, the angle between CO_2 and the surface was 63.3°, and the adsorption energy at the B8 site was −0.18 eV. Additionally, the adsorption energy of CO_2 at the B3 site was −0.13 eV, where CO_2 got adsorbed on the nearest Ti-5c site. The energy of this site was only 0.05 eV higher than of the B8 site. The optimized geometry for this configuration is shown in Fig. 1d and f; here, the distance between the lower oxygen atom of CO_2 and Ti-5c was 2.47 Å, which was shorter than at the B8 site, and the angle between CO_2 and the surface was 58.9°.

Fig. 2a illustrates the thirteen possible adsorption sites for small molecules on the anatase TiO_2 (101) surface with a V_O^{sur}. Similarly, for CO_2 adsorption at the 13 adsorption sites on the anatase (101) surface containing a V_O^{sur}, the initial configurational setup was identical to that used for the surface models with a V_O^{sub}. When CO_2 was adsorbed on a surface oxygen vacancy, the distance between the bottom oxygen atom of CO_2 and the original oxygen atom at the vacancy was 1.92 Å. The adsorption energies after relaxation are shown in Fig. 2c. Results indicated that the most stable adsorption site for CO_2 was the R2 site, with the optimized geometric structures shown in Fig. 2b and d. The most stable adsorption occurs at the top of the V_O^{sur}, where the angle between CO_2 and the surface is 77.6°, and the adsorption energy at the R2 site is −0.37 eV.

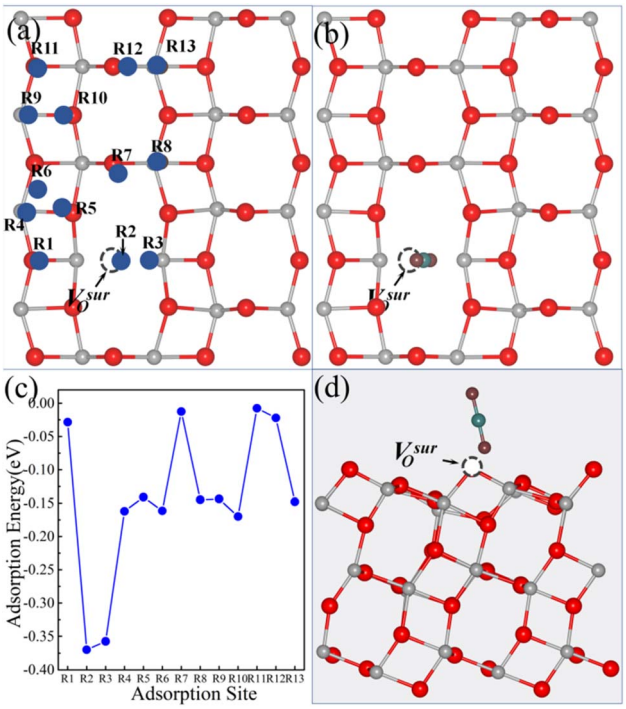

Fig. 2 (a) Top view of the anatase TiO_2 (101) surface with a V_O^{sur}, showing the thirteen possible molecule adsorption sites labeled R1–R13. Top view (b) and side view (d) of the optimized atomic structure of the CO_2-adsorbed R2 site. (c) Calculated adsorption energies of CO_2 at the thirteen different sites on the anatase (101) surface with a V_O^{sur}. In all panels, the V_O^{sur} sites are represented by black dashed spheres. In the structural diagrams, gray, red, cyan, and burgundy spheres represent titanium (Ti), surface lattice oxygen (O), carbon (C), and oxygen atoms (O) from the CO_2 molecule, respectively. The dashed circles indicate the position of the V_O^{sur}.

Our previous studies showed that a V_O^{sub} is more stable than a V_O^{sur} on a clean anatase TiO_2 (101) surface, with the surface containing a V_O^{sur} being 0.16 eV higher in total energy than the surface with a V_O^{sub}. As a result, after CO_2 adsorption on the B3 and B8 sites, the surface with the V_O^{sur} is 0.08 eV and 0.03 eV lower in total energy than the surface with the V_O^{sub}.

After CO_2 adsorption, the V_O tends to migrate from the subsurface to the surface. The calculated V_O diffusion pathway and optimized geometrical structures are shown in Fig. 3. Initially, the V_O is located in the subsurface layer, with CO_2 adsorbed on the B3 site (Fig. 3a). The oxygen atom beneath the surface (O-2c) then diffuses to the V_O^{sub} site (Fig. 3b) and forms a $V_O^{\times}$ complex (Fig. 3c). Subsequently, the surface O-2c atom diffuses to the $V_O^{\times}$ site (Fig. 3d), forming a V_O^{sur} with CO_2 adsorbed at the R2 site (Fig. 3e). The energy profiles are shown in Fig. 3f. Our calculations showed that the diffusion pathway of the V_O from the subsurface to the surface was similar to that of the clean surface.[28] The diffusion barrier of V_O on the CO_2-adsorbed surface was 0.68 eV, which was 0.18 eV lower than on the clean surface, suggesting that CO_2 adsorption promotes V_O diffusion.

Next, we examined the adsorption energy of CO on the anatase TiO_2 (101) surface with a V_O^{sub}. Thirteen possible adsorption sites and two adsorption types for CO were considered. In type 1, the CO molecule was oriented vertically with the C atom closest to the surface (Fig. 4a and c), and in type 2, the CO molecule is oriented vertically with the O atom closest to the surface (Fig. 4b). The adsorption energies of CO on the anatase TiO_2 (101) surface with a V_O^{sub} are shown in Fig. 4d. Results indicated that CO preferred to adsorb *via* type 1 configuration, where the C atom was closest to the surface, as this configuration had a lower adsorption energy than type 2 configuration. The most stable adsorption site for CO was the B3 site (type 1), and the optimized geometric structure is shown in Fig. 4a and c. The distance between CO and Ti-5c was 2.38 Å, the angle between CO and the surface was 80.1°, and the adsorption energy was −0.25 eV. In contrast, for type 2, the distance between the O atom and Ti-5c was 2.85 Å, the angle between the CO axis and the surface was 86.5°, and the adsorption energy was −0.08 eV. Furthermore, as illustrated in Fig. 4d, the adsorption energy of type 1 is consistently lower than that of type 2 at almost all equivalent adsorption sites. This thermodynamic trend clearly indicated that the CO molecule preferentially adsorbed *via* type 1 mode, making it the most stable configuration for this system.

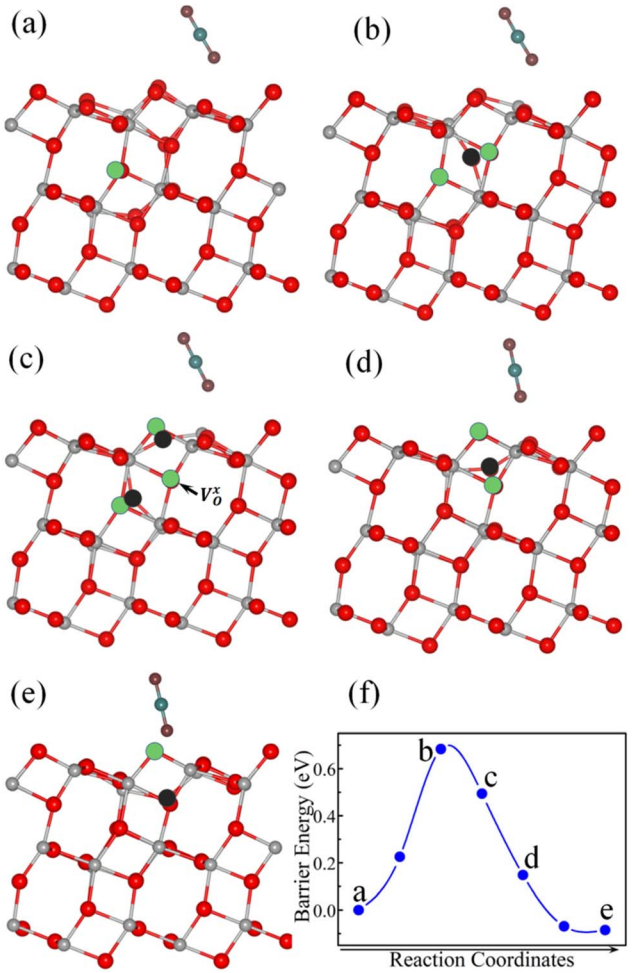

Fig. 3 Selected optimized structures (a–e) and energy profile (f) during V_O diffusion from the subsurface to the surface layer with pre-adsorbed CO_2. In the structural diagrams, gray, red, cyan, and burgundy spheres represent titanium (Ti), surface lattice oxygen (O), carbon (C), and oxygen atoms (O) from the CO_2 molecule, respectively. The black sphere represents the specific oxygen atom undergoing migration. The green circles indicate the V_O sites involved in the diffusion; in panels (b)–(d), the circles are shown to highlight the migration path. All models maintain the same stoichiometry, containing only one V_O throughout the reaction.

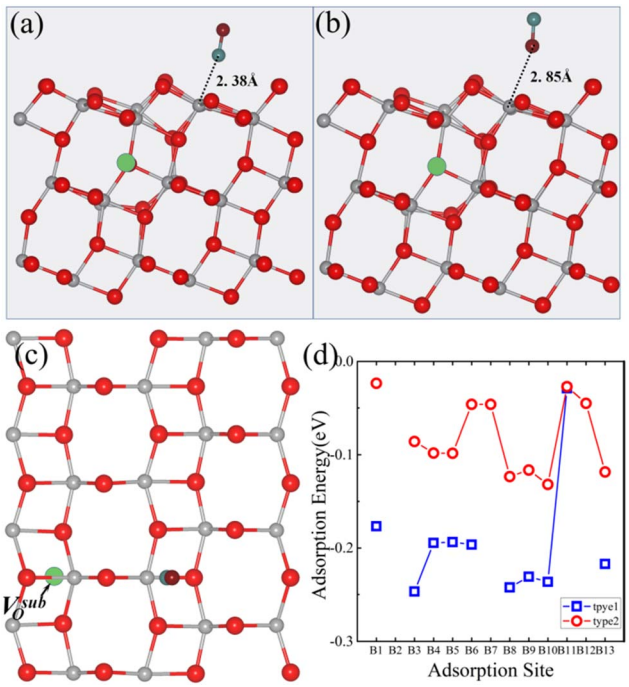

Fig. 4 (a) Top and (c) side views of the optimized atomic structure of the CO-adsorbed B3 site on the anatase TiO_2 (101) surface with a V^{sub}_O in the type 1 configuration. (b) Top view of the corresponding structure in the type 2 configuration. (d) Adsorption energies of CO on the anatase (101) surface with a V^{sub}_O. The absence of data points at certain sites in (d) indicates that CO placed at these positions is unstable and spontaneously migrates to neighboring stable sites during the relaxation process. In the structural diagrams, gray, red, cyan, and burgundy spheres represent titanium (Ti), surface lattice oxygen (O), carbon (C), and oxygen atoms (O) from the CO molecule, respectively. The green dashed circles indicate the position of the V^{sub}_O.

We also investigated the adsorption energy of CO on the anatase TiO_2 (101) surface with a V^{sur}_O. Thirteen potential adsorption sites (Fig. 2a) and two adsorption types for CO were considered. Similar to the surface with a V^{sur}_O, in type 1, the CO molecule was oriented vertically with the C atom closest to the surface (Fig. 5a and c), and in type 2, the CO molecule was oriented vertically with the O atom closest to the surface (Fig. 5b). The adsorption energies of CO on the anatase TiO_2 (101) surface with a V^{sur}_O are shown in Fig. 5d. It can be seen that, except for the R7 and R12 sites, the adsorption energies of CO in type 1 configuration were lower than those in type 2 configuration. The most stable adsorption site for CO was the R2 site in type 1 configuration, with the optimized geometry shown in Fig. 5a and c. The most stable adsorption occurred at the V^{sur}_O site, where the angle between CO and the surface was 57.8° and the adsorption energy was −0.75 eV, which was significantly larger than the energy for the same site in type 2 configuration.

Similar to CO_2, the surface with a V^{sur}_O was 0.32 eV lower in total energy than the surface with a V^{sub}_O after CO adsorption. This indicates that CO adsorption can thermodynamically reverse the relative stability of the surface with either a V^{sub}_O or V^{sur}_O. After CO adsorption on the anatase TiO_2 (101) surface with a V^{sub}_O, the relative stability of the configuration with the V^{sub}_O decreased, and the surface with the V^{sub}_O became the most stable.

The diffusion of the V_O from the subsurface to the surface with CO adsorption is shown in Fig. 6. The diffusion pathway of the V_O was similar to that observed with CO_2 adsorption. However, the diffusion barrier of the V_O on the surface with CO adsorption was only 0.36 eV, which was significantly lower than that on the clean surface by 0.50 eV. These results suggested that CO adsorption effectively promoted V_O diffusion from the subsurface to the surface layer.

Next, we studied the adsorption energy of NO on the anatase TiO_2 (101) surface with a V^{sub}_O. Similar to CO, thirteen possible adsorption sites and two adsorption types for NO were considered. In type 1, the N atom of NO was the closest to the surface

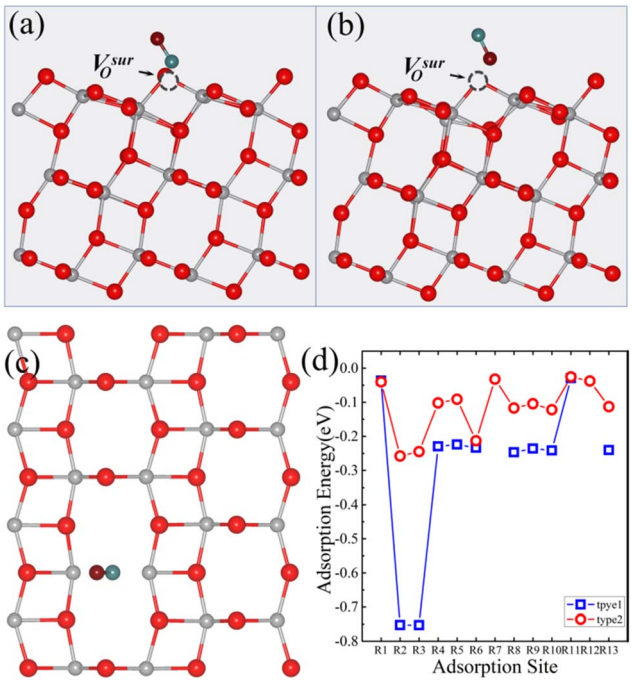

Fig. 5 (a) Top and (c) side views of the optimized atomic structure for the CO-adsorbed R2 site on the anatase TiO_2 (101) surface with a V_O^{sur} in the type 1 configuration. (b) Top view of the corresponding structure in the type 2 configuration. (d) Adsorption energies of CO on the anatase (101) surface with a V_O^{sur} for the thirteen different adsorption sites. V_O^{sur} is represented by black dashed spheres. The absence of data points at certain sites in (d) indicates that CO placed at these positions is unstable and spontaneously migrates to neighboring stable sites during the relaxation process. In the structural diagrams, gray, red, cyan, and burgundy spheres represent titanium (Ti), surface lattice oxygen (O), carbon (C), and oxygen atoms (O) from the CO molecule, respectively. The dashed circles indicate the position of the V_O^{sur}.

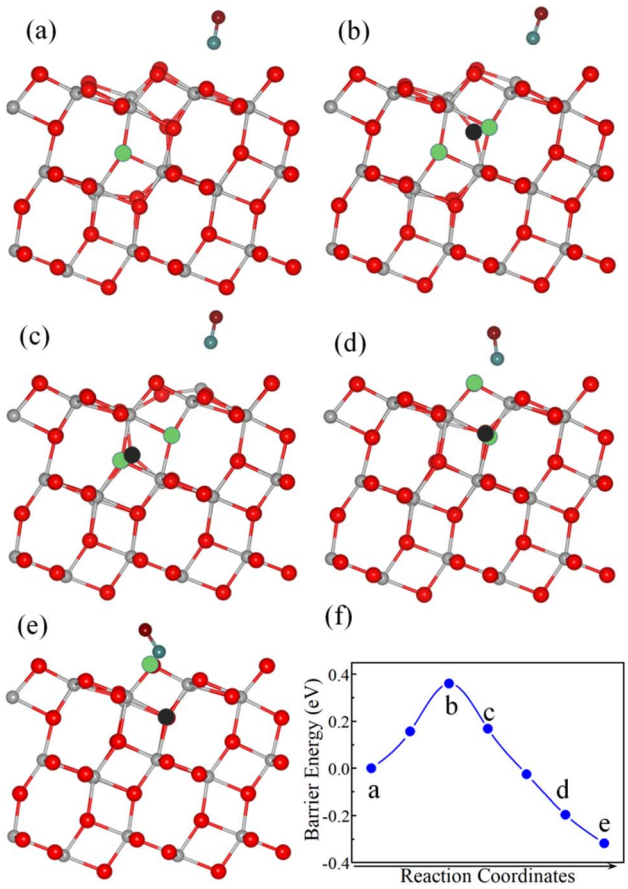

Fig. 6 Selected optimized structures (a–e) and energy profile (f) during the V_O diffusion from the subsurface to the surface layer after CO adsorption. In the structural diagrams, gray and red spheres represent titanium (Ti) and surface lattice oxygen (O) atoms and the cyan and burgundy spheres represent carbon (C) and oxygen (O) atoms from the CO molecule, respectively. The black sphere represents the specific oxygen atom undergoing migration; the green circles indicate the V_O sites involved in the diffusion. In panels (b)–(d), the circles are shown to highlight the migration path. All models have the same stoichiometry, containing only one V_O throughout the process.

(Fig. 7a and c), while in type 2, the O atom of NO was the closest to the surface (Fig. 7b). The adsorption energy of NO on the anatase TiO_2 (101) surface with a V_O^{sub} is shown in Fig. 7d. Results indicated that the B3 site was the most stable adsorption site for NO, with an adsorption energy of −0.86 eV, which was much lower than the adsorption energies of CO_2 and CO at the same site by 0.68 eV and 0.61 eV, respectively. The B3 site was located on the nearest Ti-5c site, where the distance between the N atom of NO and Ti-5c was 1.86 Å, and the angle between NO and the surface was 70.8°.

We also studied the adsorption energy of NO on the anatase TiO_2 (101) surface with a V_O^{sur}. The adsorption sites and the two identified configurations for NO are analogous to those observed for CO. Type 1 and type 2 configurations on the R2 sites are shown in Fig. 8(a–c). The adsorption energy of NO on the anatase TiO_2 (101) surface with a V_O^{sur} is shown in Fig. 8d. Results indicated that the B3 site was the most stable adsorption site for NO, with an adsorption energy of −2.60 eV, which was significantly lower than the adsorption energies of CO_2 and CO by 2.23 eV and 1.85 eV, respectively. The N atom of NO was positioned on the V_O^{sur} site, and the angle between NO and the surface was 24.4°, indicating that NO is positioned almost parallel to the surface.

After comparing the total energy following NO adsorption, we found that the surface with the V_O^{sur} is 1.58 eV lower in energy than the surface with the V_O^{sub}. This suggested that the relative stability between the surfaces with the V_O^{sub} and V_O^{sur} can be reversed through NO adsorption.

To understand the adsorption characteristics of different small molecules on the anatase TiO_2 (101) surface, we calculated the differential charge density for the stable adsorption configurations of CO_2, CO, and NO on the anatase TiO_2 (101) surface with a V_O^{sub} or V_O^{sur}, as shown in Fig. 9. When CO_2 was adsorbed on the surface with a V_O^{sub} (Fig. 9a), the charge density around the oxygen and carbon atoms of CO_2 decreased, while the charge density between the lowest oxygen atom of CO_2 and the surface increased. However, the amount of charge transfer was very small, indicating the weak adsorption of CO_2 on this

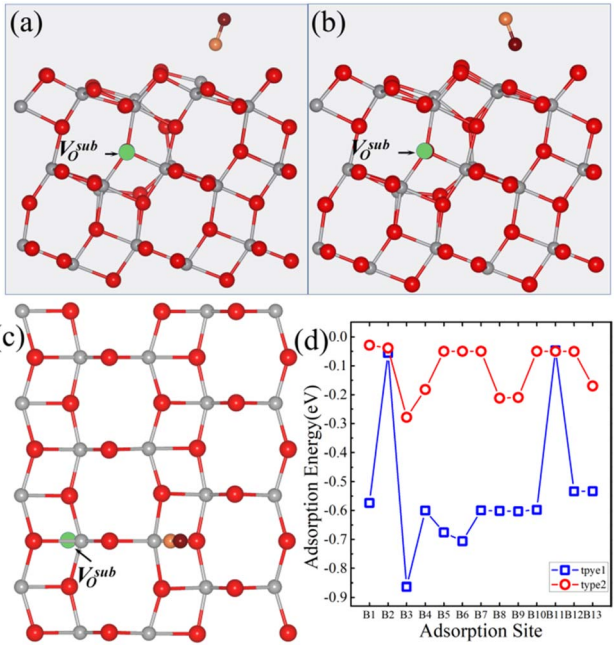

Fig. 7 (a) Top and (c) side views of the optimized atomic structure for the NO-adsorbed B3 site on the anatase TiO_2 (101) surface with a V_O^{sub} in the type 1 configuration. (b) Top view of the corresponding structure in the type 2 configuration. (d) Adsorption energies of NO on the anatase (101) surface with a V_O^{sub}. In the structural diagrams, gray, red, orange and burgundy spheres represent titanium (Ti), surface lattice oxygen (O), nitrogen (N), and oxygen atoms (O) from the NO molecule, respectively. The green dashed circles indicate the position of the V_O^{sub}.

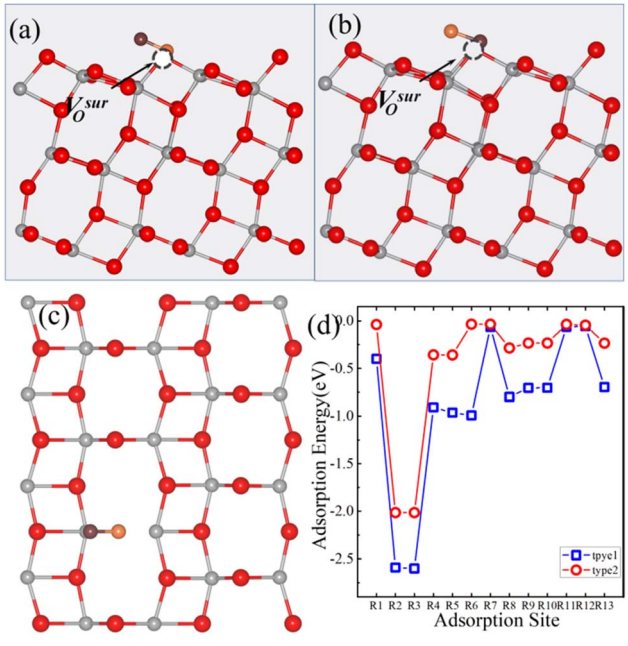

Fig. 8 (a) Top and (c) side views of the optimized atomic structure of the NO-adsorbed R2 site on the anatase TiO_2 (101) surface with a V_O^{sur} in the type 1 configuration. (b) Top view of the corresponding structure in the type 2 configuration. (d) Adsorption energies of NO on the anatase (101) surface with a V_O^{sur} for thirteen different adsorption sites. In the structural diagrams, gray, red, orange and burgundy spheres represent titanium (Ti), surface lattice oxygen (O), nitrogen (N), and oxygen atoms (O) from the NO molecule, respectively. The green dashed circles indicate the position of the V_O^{sur}.

surface. Conversely, when CO_2 was adsorbed on the surface with a V_O^{sur} (Fig. 9d), the increase in charge density between the lowest oxygen atom of CO_2 and the surface was greater than that observed on the V_O^{sub} surface, suggesting the stronger adsorption of CO_2 on the surface with a V_O^{sur}. When CO was adsorbed on the surface with a V_O^{sub} (Fig. 9b), similar to the case of CO_2 on this surface, less charge transfer occurred. However, when CO was adsorbed on a surface with a V_O^{sur} (Fig. 9e), the charge density around the surface atoms near the V_O^{sur} decreased, and a significant amount of charge accumulated between CO and the surface, indicating the strong bonding between CO and this surface. When NO was adsorbed on the surface with a V_O^{sub} (-Fig. 9c), a high charge density from the vicinity of the surface atoms accumulated between NO and the surface. The amount of charge transfer was greater than that observed for CO_2 and CO adsorption on this surface, and its adsorption energy was consequently larger. Furthermore, when NO was adsorbed on the surface with a V_O^{sur} (Fig. 9f), the angle between NO and the surface was 24.4°, indicating that NO was positioned almost parallel to the surface. A large amount of charge was accumulated not only between the N atom of NO and the surface but also between the O atom of NO and the surface, leading to a very strong bond between NO and the surface. The close agreement between the charge analysis and adsorption energy results confirmed the robustness of our findings.

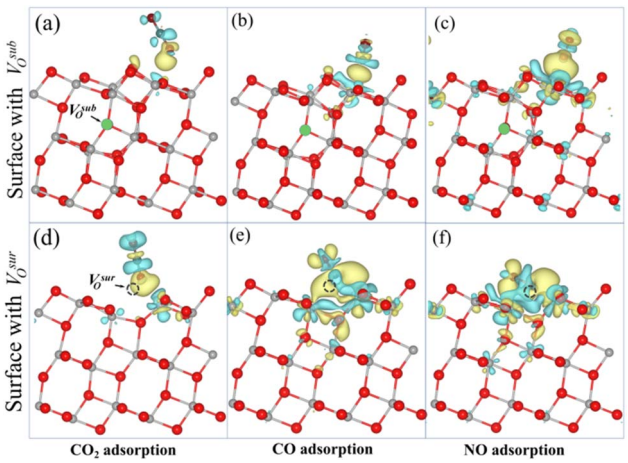

Fig. 9 Side view of the charge density difference for CO_2 (a and d), CO (b and e), and NO (c and f) molecules adsorbed on the anatase TiO_2 (101) surface with a V_O^{sub} (upper) or V_O^{sur} (lower). The iso-surfaces represent charge accumulation (yellow) and charge depletion (cyan), providing insights into the bonding mechanisms.

Conclusions

We investigated the adsorption sites and energies of CO_2, CO, and NO molecules upon their adsorption on the anatase (101)

surface with a V_O^{sub} or V_O^{sur}. On the surface with a V_O^{sub}, the most stable adsorption sites and corresponding energies are B8 (−0.18 eV), B3 (−0.25 eV), and B3 (−0.86 eV) for CO_2, CO, and NO, respectively. On the surface with V_O^{sur}, the most stable sites and energies are R2 (−0.37 eV), R3 (−0.75 eV), and R3 (−2.60 eV) for CO_2, CO, and NO, respectively. These charge analysis results closely match the adsorption energy findings, which validates the scientific soundness of our work. Importantly, we found that the surface with a V_O^{sur} is 0.03 eV, 0.32 eV, and 1.58 eV lower in total energy than the surface with a V_O^{sub} after CO_2, CO, and NO adsorption, respectively. This indicates that small molecule adsorption can thermodynamically reverse the relative stability of the surface with either a V_O^{sub} or V_O^{sur}. Additionally, we observed that the diffusion barriers of V_Os on the surface with CO_2 and CO adsorption are only 0.68 eV and 0.36 eV, respectively, which are much lower than those on the clean surface by 0.16 eV and 0.50 eV, respectively. These results suggest that CO adsorption effectively promotes V_O diffusion.

Conflicts of interest

There are no conflicts of interest to declare.

Data availability

The data supporting the findings of this study are available within the article. Additional datasets generated and analyzed during the current study are available from the corresponding author upon reasonable request.

Acknowledgements

The calculations were carried out at the High-Performance Computing Center of College of Physics and Electronic Engineering, Zhengzhou Normal University. This work was supported by the National Natural Science Foundation of China (Grant No. 12204430), the Natural Science Foundation of Henan (Grant No. 222300420378), the Technologies Research and Development Program of Henan Province (Grant No. 262102231043, 262102231046), the Key Scientific Research Project of Henan College (Grant No. 26A140016), the Innovative Research Team (in Science and Technology) in University of Henan Province (Grant No. 25IRTSTHN015), the Innovation and Entrepreneurship Training Program for college students in Henan Province (Grant No. 202312949014), and the Scientific Research and Innovation Fund for college students in Zhengzhou Normal University (Grant No. 2024009).

References

1 H. Wang, H. Qi, H. Jia, S. Li and X. Li, High quantum efficiency of hydrogen production from methanol aqueous solution with PtCu-TiO_2 photocatalysts, *Nat. Mater.*, 2023, **22**, 619.

2 O. Aldosari and U. Obaid, Unlocking the potential of TiO_2-based photocatalysts for green hydrogen energy through water-splitting: Recent advances, future perspectives and techno feasibility assessment, *Int. J. Hydrogen Energy*, 2024, **59**, 958–981.

3 W. Yuan, B. Zhu, K. Fang, X. Y. Li, J. Yang, T. S. Hansen, Y. Ou, H. Yang, J. B. Wagner, Y. Gao, Y. Wang and Z. Zhang, In situ manipulation of the active Au-TiO_2 interface with atomic precision during CO oxidation, *Science*, 2021, **371**, 517.

4 Z. Jiang, X. Xu, Y. Ma, H. S. Cho, D. Ding, C. Wang, J. Wu, P. Oleynikov, M. Jia, J. Cheng, *et al.*, Filling Metal-Organic Framework Mesopores with TiO_2 for CO_2 Photoreduction, *Nature*, 2020, **586**, 549.

5 F. Xu, K. Meng, B. Cheng, S. Wang, J. Xu and J. S. Yu, Unique, Scheme Hetero Junctions in Self-Assembled TiO_2/$CsPbBr_3$ Hybrids for CO_2 Photoreduction, *Nat. Commun.*, 2020, **11**, 4613.

6 W. Li, A. Elzatahry, D. Aldhayan and D. Zhao, Core-Shell Structured Titanium Dioxide Nanomaterials for Solar Energy Utilization, *Chem. Soc. Rev.*, 2018, **47**, 8203–8237.

7 E. J. W. Crossland, N. Noel, V. Sivaram, T. Leijtens, J. A. Alexander-Webber and H. J. Snaith, Mesoporous TiO_2 Single Crystals Delivering Enhanced Mobility and Optoelectronic Device Performance, *Nature*, 2013, **495**, 215–219.

8 R. Asahi, T. Morikawa, T. Ohwaki, K. Aoki and Y. Taga, Visible-Light Photocatalysis in Nitrogen-doped Titanium Oxides, *Science*, 2001, **293**, 269–271.

9 M. Gratzel, Photoelectrochemical Cells, *Nature*, 2001, **414**, 338–344.

10 S. Selcuk and A. Selloni, Facet-Dependent Trapping and Dynamics of Excess Electrons at Anatase TiO_2 Surfaces and Aqueous Interfaces, *Nat. Mater.*, 2016, **15**, 1107–1112.

11 U. Diebold, The Surface Science of Titanium Dioxide, *Surf. Sci. Rep.*, 2003, **48**, 53–229.

12 M. A. Henderson, The Interaction of Water with Solid Surfaces: Fundamental Aspects Revisited, *Surf. Sci. Rep.*, 2002, **46**, 1–308.

13 H. Zhang and J. F. Banfield, Understanding Polymorphic Phase Transformation Behavior during Growth of Nanocrystalline Aggregates: Insights from TiO_2, *J. Phys. Chem. B*, 2000, **104**, 3481–3487.

14 L. Kavan, M. Grätzel, S. E. Gilbert, C. Klemenz and H. J. Scheel, Electrochemical and Photoelectrochemical Investigation of Single-Crystal Anatase, *J. Am. Chem. Soc.*, 1996, **118**, 6716–6723.

15 M. Lazzeri, A. Vittadini and A. Selloni, Structure and Energetics of Stoichiometric TiO_2 Anatase Surfaces, *Phys. Rev. B: Condens. Matter Mater. Phys.*, 2001, **63**, 155409.

16 J.-Y. Liu, X.-Q. Gong, R. Li, H. Shi, S. B. Cronin and A. N. Alexandrova, (Photo)Electrocatalytic CO_2 Reduction at the Defective Anatase TiO_2 (101) Surface, *ACS Catal.*, 2020, **10**, 4048–4058.

17 M. Setvin, U. Aschauer, P. Scheiber, Y. Li, M. Hou, W. Schmid, Y. Selloni and U. Diebold, Reaction of O_2 with Subsurface Oxygen Vacancies on TiO_2 Anatase (101), *Science*, 2013, **341**, 988–991.

18 Y. Li and Y. Gao, Interplay between Water and TiO_2 Anatase (101) Surface with Subsurface Oxygen Vacancy, *Phys. Rev. Lett.*, 2014, **112**, 206101.
19 X. Lang, Y. Liang, L. Sun, S. Zhou and W.-M. Lau, Interplay between Methanol and Anatase TiO_2(101) Surface: The Effect of Subsurface Oxygen Vacancy, *J. Phys. Chem. C*, 2017, **121**, 6072–6080.
20 S. Wendt, R. Schaub, J. Matthiesen, E. Vestergaard, E. Wahlstrom, M. Rasmussen, P. Thostrup, L. Molina, E. Lagsgaard, I. Stensgaard, *et al.*, Oxygen Vacancies on TiO_2(110) and Their Interaction with H_2O and O_2: A Combined High-Resolution STM and DFT Study, *Surf. Sci.*, 2005, **598**, 226–245.
21 D. J. Shu, S. T. Ge, M. Wang and N. B. Ming, Interplay between External Strain and Oxygen Vacancies on A Rutile TiO_2(110) Surface, *Phys. Rev. Lett.*, 2008, **101**, 116102.
22 J. Zheng, Y. Lyu, R. Wang, C. Xie, H. Zhou, S. P. Jiang and S. Wang, Crystalline TiO_2 Protective Layer with Graded Oxygen Defects for Efficient and Stable Silicon-Based, *Nat. Commun.*, 2018, **9**, 3572.
23 S. M. Wu, X. L. Liu, X. L. Lian, G. Tian, C. Janiak, Y. X. Zhang, Y. Z. Lu, H. Z. Yu, J. Hu, H. Wei, *et al.*, Homojunction of Oxygen and Titanium Vacancies and its Interfacial n-p Effect, *Adv. Mater.*, 2018, **30**, 1802173.
24 Z. W. Wang and D. J. Shu, Intrinsic Interaction Between In-Plane Ferroelectric Polarization and Surface Adsorption, *Phys. Chem. Chem. Phys.*, 2019, **21**, 18680–18685.
25 Z. W. Wang, W. G. Chen, D. Teng, J. Zhang, A. M. Li, Z. H. Li and Y. N. Tang, The Effect of Strain on Water Dissociation on Reduced Rutile TiO_2(110) Surface, *RSC Adv.*, 2021, **11**, 8485–8490.
26 Y. He, O. Dulub, H. Cheng, A. Selloni and U. Diebold, Evidence for the Predominance of Subsurface Defects on Reduced Anatase TiO_2(101), *Phys. Rev. Lett.*, 2009, **102**, 106105.
27 P. Scheiber, M. Fidler, O. Dulub, M. Schmid, U. Diebold, W. Hou, U. Aschauer and A. Selloni, (Sub)Surface Mobility of Oxygen Vacancies at the TiO_2 Anatase (101) Surface, *Phys. Rev. Lett.*, 2012, **109**, 136103.
28 Z. Wang, W. Chen, D. Teng, J. Zhang, A. Li, Z. Li and Y. Tang, Interplay between H_2S and anatase TiO_2(101) surface: The effect of subsurface oxygen vacancy, *J. Phys. Chem. C*, 2022, **126**, 3939–3948.
29 J. Liu, X. Gong and A. N. Alexandrova, Mechanism of CO_2 Photocatalytic Reduction to Methane and Methanol on Defected Anatase TiO_2 (101): A Density Functional Theory Study, *J. Phys. Chem. C*, 2019, **123**, 3505–3511.
30 J. Shi, F. Yang, X. Zhao, X. Ren, Y. Tang and S. Li, Spin-polarized p-block antimony/bismuth single-atom catalysts on defect-free rutile TiO_2(110) substrate for highly efficient CO oxidation, *Phys. Chem. Chem. Phys.*, 2024, **26**, 16459.
31 M. Setvin, M. Buchholz, W. Hou and C. Zhang, A Multitechnique Study of CO Adsorption on the TiO_2 Anatase (101) Surface, *J. Phys. Chem. C*, 2015, **119**(36), 21044–21052.
32 K. M. Bulanin, A. V. Emeline, R. V. Mikhaylov, A. Y. Mikheleva, A. V. Rudakova and V. K. Ryabchuk, Dynamics of Adsorbed CO Molecules on the TiO_2 Surface under UV Irradiation, *J. Phys. Chem. C*, 2023, **127**, 11005–11013.
33 C. Fu, H. Xu, L. Wu, Z. Zhang and W. Huang, X-ray-Induced CO_2 Formation via CO Reaction with TiO_2 at Cryogenic Temperature, *J. Phys. Chem. Lett.*, 2021, **12**, 9741–9747.
34 Z. Wang, G. Lv, C. Zhang and X. Sun, Catalytic Oxidation Mechanism of NO to HNO_3 on TiO_2 (101) and (001) Surfaces and the Influence Factors on NO Removal: A DFT Study, *J. Environ. Chem. Eng.*, 2021, **9**, 104643.
35 L. Mino, M. Cazzaniga, F. Moriggi and M. Ceotto, Elucidating NOx Surface Chemistry at the Anatase (101) Surface in TiO_2 Nanoparticles, *J. Phys. Chem. C*, 2023, **127**, 437–449.
36 J. P. Perdew, K. Burke and M. Ernzerhof, Generalized Gradient Approximation Made Simple, *Phys. Rev. Lett.*, 1996, **77**, 3865–3868.
37 F. Allegretti, S. O'Brien, M. Polcik, D. I. Sayago and D. P. Woodruff, Adsorption Bond Length for H_2O on TiO_2(110): A Key Parameter for Theoretical Understanding, *Phys. Rev. Lett.*, 2005, **95**, 226104.
38 G. Kresse and D. Joubert, From Ultrasoft Pseudopotentials to the Projector Augmented-Wave Method, *Phys. Rev. B: Condens. Matter Mater. Phys.*, 1999, **59**, 1758–1775.
39 P. E. Blöchl, Projector Augmented-Wave Method, *Phys. Rev. B: Condens. Matter Mater. Phys.*, 1994, **50**, 17953–17979.
40 G. Mills, H. Jonsson and G. K. Schenter, Reversible Work Transition State Theory: Application to Dissociative Adsorption of Hydrogen, *Surf. Sci.*, 1995, **324**, 305–337.
41 V. Wang, N. Xu, J.-C. Liu, G. Tang and W.-T. Geng, *Comput. Phys. Commun.*, 2021, **267**, 108033.
42 C. Freysoldt, B. Grabowski, T. Hickel, J. Neugebauer, G. Kresse, A. Janotti and C. G. Van de Walle, *Rev. Mod. Phys.*, 2014, **86**, 253–305.